Cell Systems

Article

Design, mutate, screen: Multiplexed creation and arrayed screening of synchronized genetic clocks

Graphical abstract

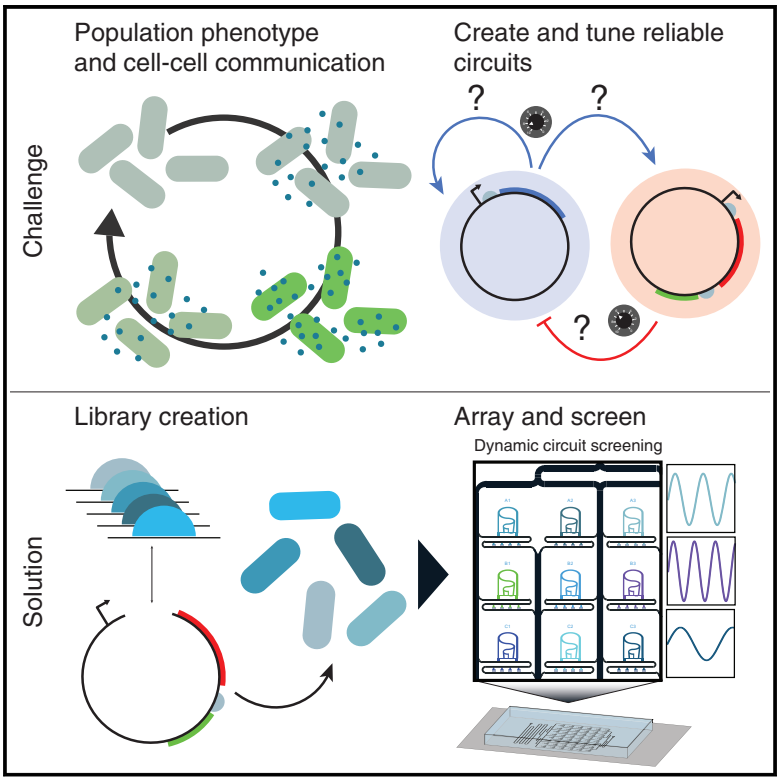

Authors

Andrew Lezia, Nicholas Csicsery, Jeff Hasty

Correspondence

hasty@bioeng.ucsd.edu

In brief

A multiplexed-microfluidic platform and strategy for screening mutant libraries for dynamic, population-level phenotypes are developed. Using this technology, variants of two oscillator circuits are created and screened for differences in their dynamics.

Highlights

- A microfluidic device is developed for arrayed library screening of dynamic phenotypes
- Variants of an oscillatory, synchronized cell lysis circuit are created and screened
- A transcription-based synchronized oscillator is optimized by mutation and screening
- The utility of mutant library screening even when rational design tools exist is shown

Lezia et al., 2022, Cell Systems *13*, 365–375
May 18, 2022
https://doi.org/10.1016/j.cels.2022.02.005

CellPress

Cell Systems

CellPress

Article

Design, mutate, screen: Multiplexed creation and arrayed screening of synchronized genetic clocks

Andrew Lezia,[1,4] Nicholas Csicsery,[1,4] and Jeff Hasty[1,2,3,*]
[1]Department of Bioengineering, University of California, San Diego, La Jolla, CA, USA
[2]Molecular Biology Section, Division of Biological Sciences, University of California, San Diego, La Jolla, CA, USA
[3]BioCircuits Institute, University of California, San Diego, La Jolla, CA, USA
[4]These authors contributed equally
*Correspondence: hasty@bioeng.ucsd.edu
https://doi.org/10.1016/j.cels.2022.02.005

SUMMARY

A major goal in synthetic biology is coordinating cellular behavior using cell-cell interactions; however, designing and testing complex genetic circuits that function only in large populations remains challenging. Although directed evolution has commonly supplemented rational design methods for synthetic gene circuits, this method relies on the efficient screening of mutant libraries for desired phenotypes. Recently, multiple techniques have been developed for identifying dynamic phenotypes from large, pooled libraries. These technologies have advanced library screening for single-cell, time-varying phenotypes but are currently incompatible with population-level phenotypes dependent on cell-cell communication. Here, we utilize directed mutagenesis and multiplexed microfluidics to develop an arrayed-screening workflow for dynamic, population-level genetic circuits. Specifically, we create a mutant library of an existing oscillator, the synchronized lysis circuit, and discover variants with different period-amplitude characteristics. Lastly, we utilize our screening workflow to construct a transcriptionally regulated synchronized oscillator that functions over long timescales. A record of this paper's transparent peer review process is included in the supplemental information.

INTRODUCTION

Over the last decade, synthetic biologists have increasingly focused on creating genetic circuits to control complex, population-level behavior (Song et al., 2011). By harnessing cell-cell communication systems, such as naturally occurring quorum sensing (QS) modules in bacteria, researchers have created circuits that synchronize behaviors, such as genetic oscillations, across thousands of cells (Chen et al., 2015; Prindle et al., 2011). Population-level synthetic gene circuits have been applied in many areas, such as living-therapeutics where cell-cell communication has been used to engineer population-control mechanisms that decrease the chance of systemic inflammatory responses to engineered bacteria (Din et al., 2016). In recent years, circuits for cell-cell communication have helped create microbial consortia composed of distinct strains that mimic naturally occurring ecosystems where metabolic pathways are distributed across different organisms (Grandel et al., 2021). An increased interest in population-level gene circuits has brought new challenges in circuit design and testing. Whereas the ability to screen dynamic single-cell circuits has improved dramatically in the last few years, there has been less progress on the methods to screen for complex, population-level phenotypes.

Two approaches have greatly facilitated genetic circuit creation: (1) rational "plug and play" methods and (2) evolutionary "design then mutate" strategies (Haseltine and Arnold, 2007). In the "plug and play" method, researchers choose well-characterized genetic components to rapidly engineer a circuit with the desired behavior predicted by a computational model (Nielsen et al., 2016). Although the principles of abstraction and standardization afforded by this method are alluring, the context-dependent function of genetic parts often prevents this method from reaching the same precision as in other engineering fields (Del Vecchio, 2015; Karamasioti et al., 2017). Conversely, directed evolution or "design then mutate" methods for gene circuit construction take a different approach. In this method, mathematical models guide the selection of key circuit components (e.g., promoters, ribosome binding sites [RBSs], and operators) to mutate and create large libraries of variants, which are then screened (Hasty, 2002; Yokobayashi et al., 2002). Methods to create large, targeted mutant libraries have improved vastly, now allowing researchers to simultaneously mutate multiple genetic targets at once (Gallagher et al., 2014; Liu and Naismith, 2008; Zeng et al., 2018), use host organisms to mutate the desired target *in vivo* (Alexander et al., 2014; Esvelt et al., 2011; Halperin et al., 2018), and rapidly assemble many pieces of DNA in single

reactions (Gibson et al., 2009; Weber et al., 2011). Site-directed mutagenesis (SDM) techniques in particular have made the creation of precisely targeted mutant libraries easy, inexpensive, and fast (Jain and Varadarajan, 2014). In general, a combination of rational design and directed evolution is ideal because it takes advantage of the existing biological knowledge while also acknowledging the remaining gaps in understanding. Regardless of the method chosen to get from conceptual design to functional circuit, the ability to rapidly screen circuit variants for a desired phenotype is paramount.

Presently, devising methods to screen variants from large libraries is more challenging than creating the libraries (Schaerli and Isalan, 2013). As researchers continue to study more complex, time-dependent cellular behaviors, there is a need for technologies that take advantage of the high spatiotemporal information provided by live-cell, time-lapse microscopy while maintaining the ability to identify and isolate unique variants from large libraries. New advances in library screening have done just this: improving the throughput of screening while maintaining the ability to link genotype-phenotype relationships in interesting variants. Two separate groups recently developed related imaging-based methods for observing complex phenotypes in large pool-synthesized strain libraries and connecting the observed phenotypes with the underlying cell genotypes (Emanuel et al., 2017; Lawson et al., 2017). Both these methods separate phenotype observation and genotype determination into two steps. After time-lapse imaging is used to observe complex phenotypes among library members either adhered to a cover slip or continuously cultured in a mother machine-like microfluidic device, the cells are fixed and multiple rounds of fluorescent *in situ* hybridization (FISH) are performed to detect unique RNA bar codes expressed by each strain. Since each RNA bar code is associated with a known, unique genetic perturbation, bar code determination for a given strain directly connects genotype and phenotype, something that has typically been challenging for large, pooled-strain libraries. In an impressive demonstration of their workflow, Lawson et al. determined how 235 different CRISPR interference knockdowns impacted the coordination between replication and division cycles in *E. coli* (Camsund et al., 2020).

Another group recently developed a method to isolate single cells after time-lapse microscopy (SIFT) using optical trapping (Luro et al., 2020). They screened a large library of precise synthetic gene oscillators and uncovered variants spanning a 30-fold range of average periods. In this method, since cells can be retrieved after long-term imaging of dynamic behavior in a microfluidic device, cells with interesting phenotypes can be propagated and sequenced. Notably, tens of thousands of cell lineages can be screened per day with this technique. Although both *in situ* genotyping and optical trapping of strains from pooled-strain libraries dramatically improve screening for dynamic phenotypes at the single-cell level, these technologies are currently incompatible for screening population-level genetic circuits that rely on cell-cell communication.

In this work, we have addressed the gap in techniques to screen mutant libraries of population-level genetic circuits for dynamic phenotypes. We built upon previously developed multiplexed microfluidic platforms for arrayed cell library screening to simultaneously culture dozens of unique *E. coli* populations from large mutant libraries (Graham et al., 2020). Our technique enabled us to rapidly array potentially up to 48 distinct strains on a microfluidic device directly from liquid culture. Using this arrayed-strain microfluidic culture system, we developed a workflow for quantitatively screening libraries of gene circuits with complex phenotypes only seen at the population level. We used this workflow to tune the dynamics of an existing oscillator, the synchronized lysis circuit (SLC) (Din et al., 2016), and uncovered new principles regarding its regulation. Additionally, we developed a new synchronized gene oscillator and demonstrated how we are able to improve the circuit by combining computational modeling with our screening pipeline. The final oscillator we developed exhibits robust and tunable oscillations over long time scales. Overall, this work demonstrates the power of directed mutagenesis to supplement rational circuit design and illustrates how arrayed, multistrain microfluidics can improve the ability to screen dynamic phenotypes at the population level.

RESULTS

Overview of directed evolution approach for synthetic oscillator creation and tuning

We sought to develop a system for constructing and tuning dynamic, population-level gene circuits by directed mutagenesis and screening (Figure 1). In this work, we focus on tuning and creating QS-based oscillator circuits in *E. coli* because they (1) exhibit complex, time-varying phenotypes that can be difficult to predict and monitor; (2) have many dynamic parameters that can be tuned (e.g., period, amplitude, and prominence); and (3) are increasingly being tested for real-world applications. We began by creating targeted mutant libraries of a genetic circuit using SDM. We utilized deterministic modeling of circuit dynamics to help guide the choice of circuit elements to mutate. Following library creation, we screened strains for interesting phenotypes in both well plate-based batch culture and microfluidic-based continuous culture. Batch culture screening approaches permit rapid screening of many variants for significant phenotype differences but are insufficient for observing dynamic phenotypes seen only in continuous culture where the metabolic state of the cell population is relatively constant (Bull, 2010). Thus, after an initial library screen in 96-well plates, we deployed a high-throughput, multistrain microfluidic device to further screen interesting library members.

The multistrain device was adapted from a previous design in which a single inlet-outlet system fed a manifold array of 2,176 cell traps (Graham et al., 2020). For an improved compatibility with liquid cultures instead of solid colonies (liquid cultures have a greater tendency to wick and spread through channels), the spacing between spotting regions where cells are deposited was increased from 1.125 to 2 mm (Figure S1). The final PDMS-based device consists of a 6 × 8 array of cell-trapping regions that are loaded with liquid bacterial cultures by acoustic droplet ejection using a Labcyte Echo 550 prior to bonding the device to a glass slide or cover slip. Each position features four smaller cell traps downstream of the large trapping region that serve as regions of interest (ROIs) for tracking population dynamics in fluorescent and transmitted light channels. With this device, up to 48 distinct positions can be loaded with a unique *E. coli* strain, each

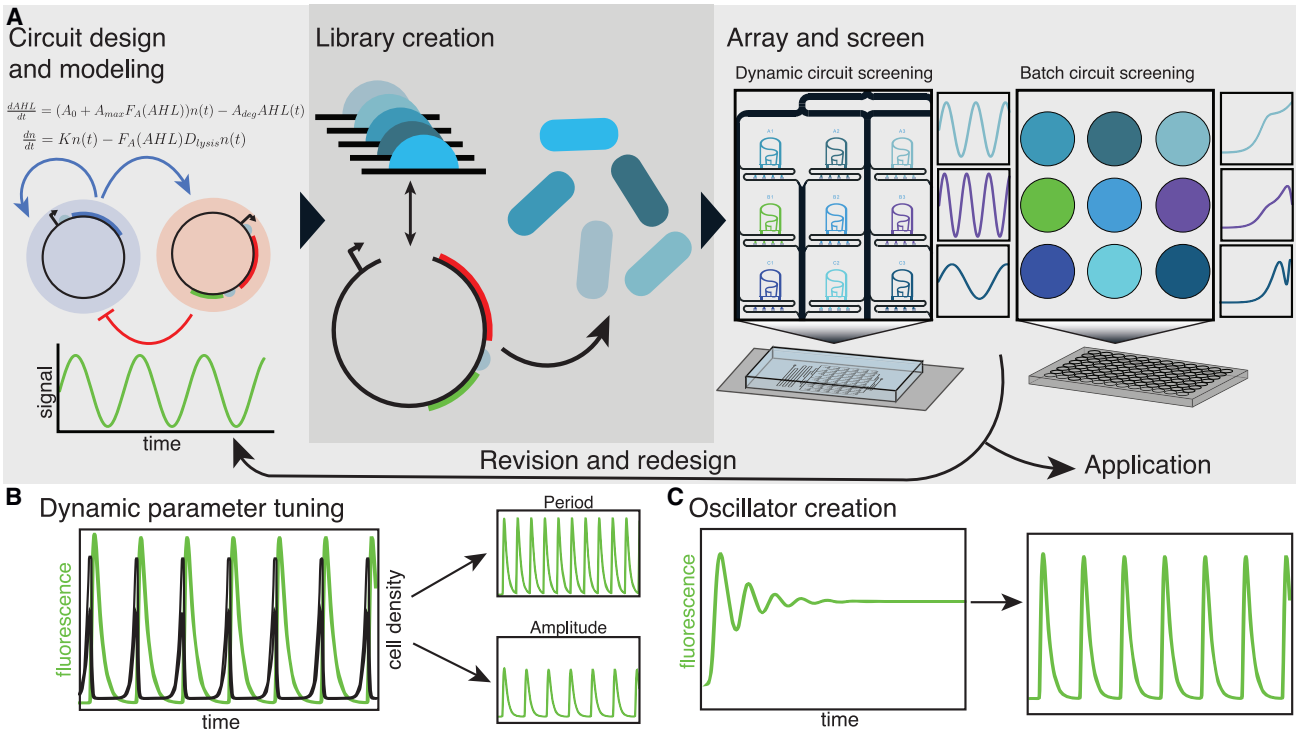

Figure 1. Synthetic oscillator creation and tuning through directed mutagenesis and screening

(A) Overview of gene circuit creation and screening workflow. Mathematical modeling of circuit dynamics helps to identify parameters to target in order to improve or modify circuit behavior. Large libraries of a given circuit are quickly constructed via site-directed-mutagenesis (SDM). High-throughput, multistrain microfluidic devices permit dynamic phenotype screening to supplement and improve upon traditional batch-culture methods of circuit screening. Circuit variants with desired or interesting behavior can be used for real-world applications, used to better inform circuit models, or placed through another cycle of mutagenesis and screening to further improve behavior.

(B) The gene circuit library construction and screening workflow developed here can be used to tune the behavior of an existing oscillator circuit.

(C) The system can also aid in the construction of new genetic circuits such as oscillators synchronized at the population level.

housing a continuous culture for multiple days where media composition and flow rate are precisely controlled. The high spatiotemporal resolution data from variants can be used to improve circuit models and inform design considerations for relevant applications.

Tuning the oscillatory dynamics of a SLC by directed mutagenesis

To demonstrate the ability of our system to tune circuit dynamics via directed mutagenesis and screening, we worked with a single plasmid version of a previously developed synthetic gene oscillator, the SLC (Din et al., 2016). Bacteria transformed with the SLC have been used to release therapeutics in solid tumors (Din et al., 2016; Sepich-Poore et al., 2021; Wu et al., 2019; Zhou et al., 2018), and the ability to tune the circuit dynamics could improve the utility of this circuit for cancer therapy. In the SLC, the expression of the LuxI protein, and subsequent production of the QS autoinducer N-Acyl homoserine lactone (AHL), generates synchronized positive feedback in a colony of isogenic cells. The positive activation of the pLux promoter in turn drives negative feedback via the expression of the lysis protein, E, from phage φX 174, causing synchronized lysis of the colony. A few cells in the population are able to survive the lysis event and continue growing, perpetuating cycles of growth, gene expression, and mass lysis (Figure 2A).

We generated a mutant library of the SLC by randomizing five base pairs in the RBS upstream of the lysis protein leading to as many as 1,024 unique circuit variants (Figure 2A). We chose to create a library significantly larger than the maximum throughput of our microfluidic device to increase the probability that transformants selected at random would all have different RBS sequences. Altering the strength of the RBS preceding the lysis gene affects the translation rate for the lysis protein, which potentially alters the oscillatory dynamics by modulating the negative feedback component of the circuit. We hypothesized that strains with a stronger RBS driving the lysis gene would lyse more rapidly upon reaching a threshold population size, leading to higher frequency oscillations compared with strains with weaker RBSs.

We randomly selected 24 members from the SLC library for screening. We cultured these strains in a 96-well plate and monitored their lysis dynamics using a TECAN (Zurich, Switzerland) microplate reader. For the 24 strains examined in batch, we saw differences in the presence and magnitude of lysis events and green fluorescent protein (GFP) expression immediately before a lysis event (Figure 2B). While differences in cell population dynamics and GFP fluorescence can be coarsely ascertained from

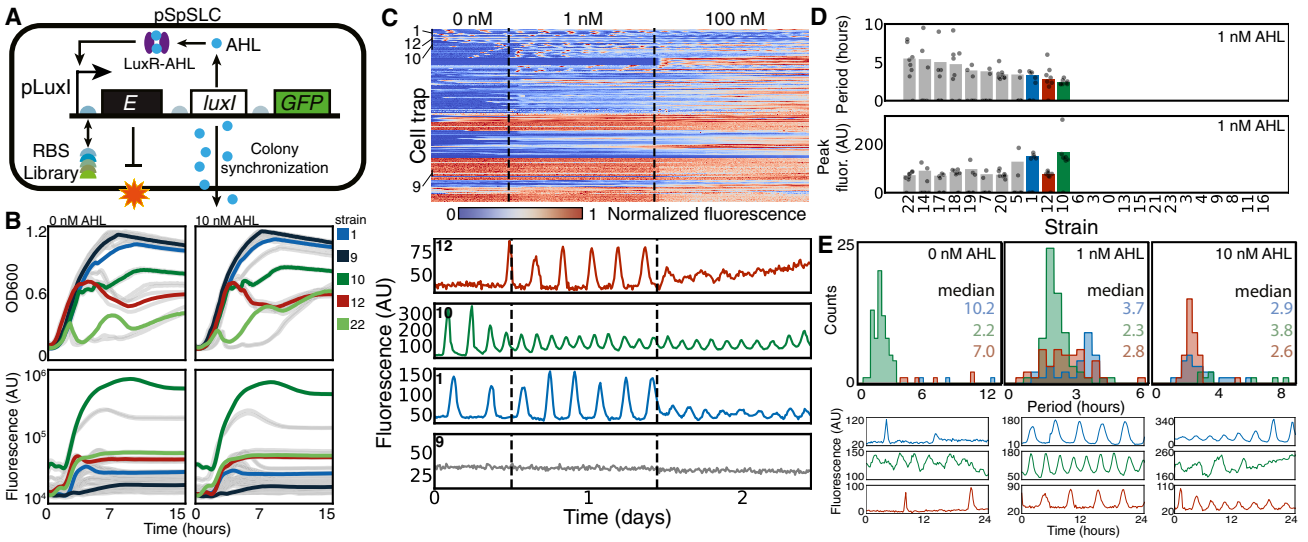

Figure 2. Screening of synchronized lysis circuit (SLC) library strains

(A) A single-plasmid synthetic oscillator (pSpSLC) was developed, with AHL production from the LuxI protein as a cell-synchronized positive feedback mechanism and cell lysis as negative feedback. A library was created by randomizing five bases in the RBS upstream of the lysis protein gene, E.

(B) When screened in batch culture, the library strains exhibit a range of growth, lysis, and GFP expression dynamics.

(C) Twenty-four library members were screened on a 48-strain microfluidic device and subjected to temporal changes in the background AHL concentration. Different, dynamic fluorescent phenotypes were observed across these 24 strains, with four examples being shown. In the heat map, fluorescence (AU) of each strain was linearly scaled between 0 and 1 relative to itself.

(D) Extracted parameters, oscillation period, and peak fluorescence of 24 oscillator strains under 1-nM AHL. Eight cell traps were evaluated for each strain, with each point representing the measured value for a single trap. Non-oscillating cell traps were reported as zero, with bars representing the mean of the oscillating traps.

(E) Peak-peak interval histograms for three library strains under different AHL concentrations, with 8 distinct cell traps evaluated for each strain. Representative GFP time traces for each strain at the specified AHL concentration are shown.

the batch culture data, sustained SLC oscillations are typically seen only in continuous culture, necessitating the use of multiplexed microfluidics for dynamic parameter screening.

In parallel with the batch culture experiments, the 24 selected library members were screened on a 48-position multiplexed device using a previously described custom optical assembly (Graham et al., 2020). Both fluorescence and transmitted light images were collected every 10 min, with fluorescence used as the primary output to quantify oscillator dynamics. Although 48 unique strains can grow in the device simultaneously, screening only 24 members allowed for additional replicates on the chip (8 small cell trap ROIs per strain). Experiments were started on Luria Bertani broth media with 0 nM AHL for 12 h during initial trap filling and then subjected to varying background concentrations of AHL over several days to survey oscillatory dynamics. Clustering of all cell traps revealed an abundance of phenotypes, predominantly "broken" oscillators with no fluorescent oscillatory dynamics, but also several working oscillators (Figure 2C). Four strains are highlighted in Figure 2C, showing three working oscillators that activate under different AHL concentrations and have differences in their period and amplitude across conditions. Dynamic parameters (period and peak fluorescence) were extracted for all 24 strains at 1 nM AHL to quantitatively demonstrate the variety of oscillators discovered by library screening (Figure 2D). To further characterize the three working oscillators highlighted in Figure 2C ($pSpSLC_0$, $pSpSLC_{10}$, and $pSpSLC_{12}$), peak-peak interval histograms for these strains were constructed (Figure 2E). Analysis of these oscillation frequencies at varied AHL concentrations reveals ideal conditions for each oscillator, with $pSpSLC_{10}$ exhibiting more consistent oscillations at 1 nM AHL and $pSpSLC_{12}$ oscillating more consistently at 10 nM AHL. For strain $pSpSLC_{12}$, oscillations are sparse at 0 nM of AHL, regular at 1 and 10 nM, with frequency increasing at higher concentrations, and absent at 100 nM (Figures 2C and 2E). The trend of more frequent oscillations with increasing exogenous AHL concentration matched the modeling results obtained using a deterministic model of the SLC (Figure S2A).

To better understand how changes to the lysis gene RBS led to different oscillator dynamics, we investigated two strains in more detail. Specifically, we looked at the original oscillator ($pSpSLC_0$) used to build the library, which exhibited frequent oscillations with little to no GFP production before lysis and compared it with library strain 10 ($pSpSLC_{10}$), which exhibited slower oscillations and high GFP expression before each lysis event (Figures 3A and 3B; Videos S1 and S2). To directly characterize how the different RBSs affected population lysis in response to AHL, we reconstructed the strains without the positive feedback component, *luxI* (Figure S2B). In batch culture, we then grew the strains under varying AHL concentrations to generate a lysis dose-response curve for each RBS (Figures 3C, 3D, and S2B). We found that the original strain with higher frequency oscillations had a much lower EC_{50} than the lower frequency library strain, strongly suggesting that $pSpSLC_0$ had a higher translation initiation rate for the lysis gene. Using a previously developed

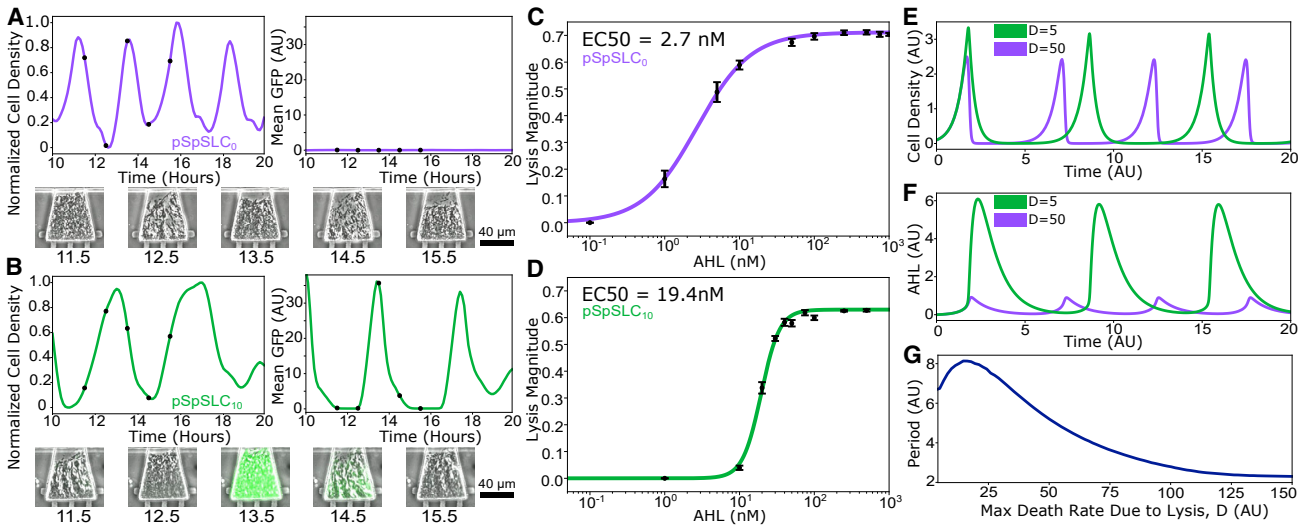

Figure 3. Comparison of SLC library strains with varying lysis strengths reveals differences in the gene expression dynamics

(A) GFP and cell density time traces for the original single plasmid SLC ($pSpSLC_0$) grown in the multistrain microfluidic device with accompanying microscope images of one microfluidic trap for specific time points.

(B) GFP and cell density time traces for SLC library strain 10 ($pSpSLC_{10}$) grown in the multistrain microfluidic device with accompanying microscope images of one microfluidic trap for specific time points.

(C) Lysis dose-response curve for $pSpSLC_0$. Error bars represent standard deviation of three separate lysis measurements.

(D) Lysis dose-response curve for $pSpSLC_{10}$. Error bars represent standard deviation of three separate lysis measurements.

(E) SLC modeling results showing how changing the maximum death rate due to lysis, D, impacts oscillatory population dynamics.

(F) SLC modeling results showing how changing the maximum death rate due to lysis, D, impacts AHL concentration dynamics.

(G) Modeling results showing how the period of lysis oscillations changes with the parameter D.

deterministic model of the lysis circuit dynamics (Scott et al., 2017), we confirmed that the period of oscillations is generally inversely correlated with the strength of expression for the lysis gene (Figures 3E, 3F, and 3G). Additionally, this model showed that the peak AHL (and GFP) production immediately preceding a lysis event decreased as the expression strength of the lysis gene was increased (Figures 3F and S2C). This prediction from the model agreed with our experimental results where the library strain with the weaker RBS driving the lysis gene exhibited substantially more GFP expression preceding lysis.

The usefulness of *in situ* screening with a "design then mutate" approach was further demonstrated when investigating rational design tools, such as the RBS calculator developed by Espah Borujeni et al. (2014). For the $pSpSLC_0$ RBS and the $pSpSLC_0$ RBS sequences, the RBS calculator predicted lysis protein translation rates of 1,957 and 1,460, respectively. Despite these small differences in predicted translation rates, within the reported margin of error for the calculator (Reis and Salis, 2020), the experimentally measured lysis dose-response curves for the two RBS variants demonstrated significant differences in lysis gene expression strength, with the $pSpSLC_0$ having an EC_{50} of 2.7 nM and the $pSpSLC_{10}$ having an EC_{50} of 19.4 nM (Figures 3C and 3D). To further examine these RBSs, they were placed in a circuit with a simpler phenotype: constitutive expression of sfGFP on a low-copy-number plasmid. In this GFP-expressing circuit, the $pSpSLC_0$ RBS sequence led to an approximately 10-fold increase in GFP expression relative to the $pSpSLC_0$ RBS sequence, whereas the RBS calculator predicted a lower translation rate (8,839) for the $pSpSLC_0$ RBS than that for the $pSpSLC_{10}$ RBS (14,049) (Figure S5A). It is well documented that the protein coding component of an mRNA transcript can affect translation initiation, leading to the same RBS sequence yielding different translation rates depending on the downstream sequence (Napolitano et al., 2016; Salis et al., 2009). Nonetheless, our characterization of these RBS sequences in an AHL-inducible lysis circuit and a constitutive GFP-expressing circuit yielded similar results for their relative strength. Thus, in this case, we found *in situ* screening to be more useful than the existing rational design tools, particularly in the context of the lysis circuit where small changes in expression level can lead to large changes in the observed phenotype due to the complex mechanism of the lysis protein (Bernhardt et al., 2000). Together, these results highlight the importance of screening for desired circuit properties, even for libraries where circuit components can be rationally designed to a degree, especially in the context of complex phenotypes such as the population-level oscillations of the SLC.

Our results here demonstrate the importance of considering the relative RBS strength for the lysis gene in the SLC. In therapeutic applications using this circuit (Din et al., 2016), it may be desirable to have the production of a therapeutic gene driven by the same pLux promoter as the lysis gene. Here, we demonstrate the importance of considering the relative expression strength for the lysis gene and a therapy gene in this scenario. If the lysis gene translation initiation rate far exceeds that of the therapy gene, the engineered cells may exhibit robust cycles of growth and lysis without releasing a significant amount of therapeutics, akin to the case for the original SLC strain where there was little to no GFP production preceding each lysis event.

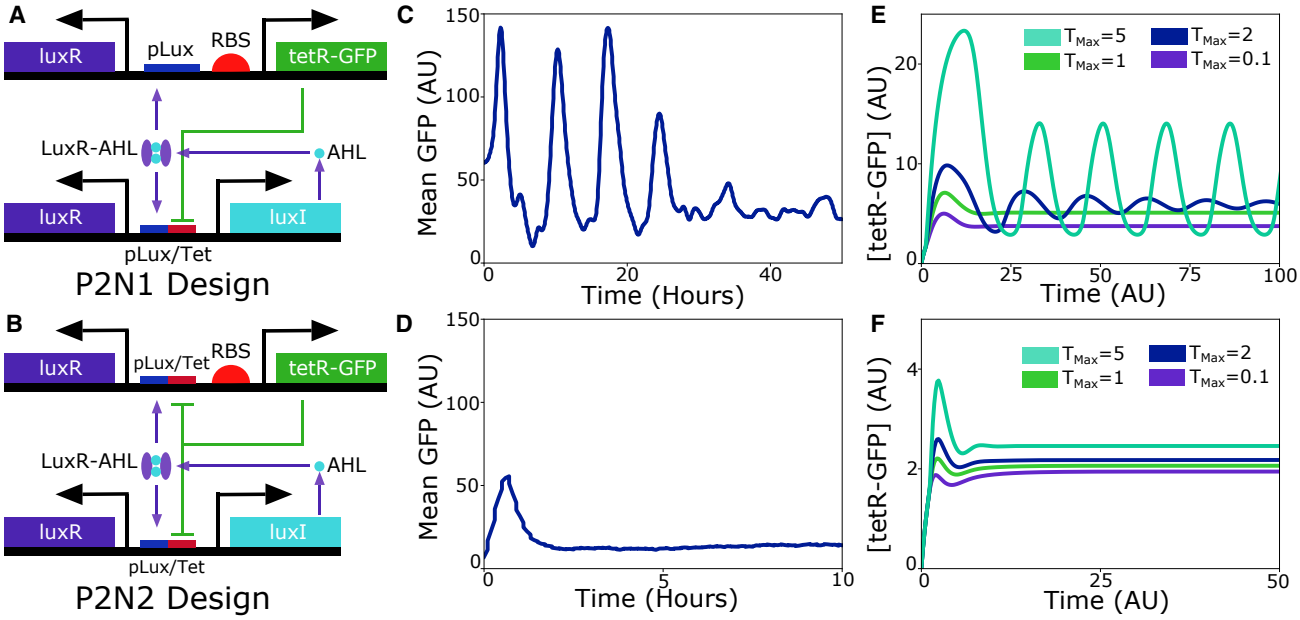

Figure 4. Comparison between P2N1-Tet and P2N2-Tet circuit topologies

(A) Circuit diagram for the P2N1-Tet design.

(B) Circuit diagram for the P2N2-Tet design.

(C) Representative mean GFP time trace for the first implementation of the P2N1 oscillator design in a cell trap with area of 0.81E−2 mm^2 at an aTc concentration of 50 ng/mL.

(D) Representative time trace for first implementation of the P2N2-Tet oscillator design in a cell trap with area of 0.81E−2 mm^2 at an aTc concentration of 50 ng/mL.

(E) Modeling results for P2N1-Tet design with delay parameter set to one for varying maximal expression levels of TetR.

(F) Modeling results for P2N2 design with delay parameter set to one for varying maximal expression levels of TetR (T_{Max}).

Creation of a transcriptionally regulated synchronized gene oscillator circuit via directed mutagenesis and screening

Beyond tuning the oscillatory phenotypes of an *existing* oscillator, such as the SLC, we sought to further show the utility of our screening workflow for optimizing *new* population-level genetic circuits with complex dynamics. Although tuning the dynamic behavior of a circuit is a common goal in synthetic biology, it is often difficult to create a circuit that displays the desired behavior predicted by a model in the first place, especially for circuit designs where the desired dynamics might exist only for a small number of parameters. We chose to implement a synchronized gene oscillator design consisting of coupled positive and negative feedback loops using only QS molecule production and simple transcriptional regulation.

Although a plethora of QS-mediated, population-level oscillators have been previously developed in bacteria, most do not exclusively use transcriptional repression as a negative feedback mechanism, often relying on QS molecule degradation proteins or in the case of the SLC, the destruction of cellular components (Baumgart et al., 2017; Chen et al., 2015; Danino et al., 2010; Din et al., 2016). In the case of population-level oscillators, using only transcriptional repressors may be particularly applicable to QS systems for which QS molecule degradation enzymes have not been identified. In a recent study, Chen et al. employed the repressor LacI as a negative feedback mechanism in conjunction with the QS molecule degradation enzyme AiiA in a multistrain oscillator (Chen et al., 2015). For this system, they explored different positive and negative feedback motifs, notably finding that a design with 2 negative and 2 positive feedback links (P2N2) was more robust than a design with a single negative feedback link (P2N1). Instead, we sought to further explore these motifs in a single-strain system that could require fine parameter tuning to improve, or even see, oscillatory dynamics.

To begin with, we created two versions of the oscillator circuit with slightly different topologies, similar to Chen et al. (Figures 4A and 4B). The first version, P2N1-Tet (no negative autoregulation), uses two AHL inducible promoters: pLuxTet, which is activated by the LuxR-AHL complex and repressed by the tetracycline repressor protein, TetR, and pLux, which is only activated by LuxR-AHL. pLuxTet drives the production of LuxI, which synthesizes AHL and drives positive feedback. pLux drives the production of fluorescently tagged TetR, which represses pLuxTet. As each cell accumulates high levels of TetR, the pLuxTet promoter becomes inactivated, leading to a steady decline in AHL because it is removed from the population by fluid flow. The second circuit topology, P2N2-Tet (with negative autoregulation), is identical to P2N1-Tet except that the TetR-repressible pLuxTet promoter is used for the expression of both LuxI and TetR. TetR was chosen as the transcriptional repressor because it binds the TetO operator as a dimer (Orth et al., 2000) and is typically modeled with a lower hill coefficient than LacI, which binds LacO as a tetramer and can also be involved in DNA looping

(Rutkauskas et al., 2009). Previous research on delayed-negative feedback oscillators suggests that high nonlinearity (i.e., cooperativity) in repressor binding increases the parameter range for which oscillatory behavior is observed (Ferrell and Ha, 2014; Lepzelter et al., 2010). Thus, for designs with lower repressor binding cooperativity, such as the TetR design explored here, it may be important to screen mutant libraries for circuits that oscillate.

Initially, we wanted to characterize a first implementation of each oscillator design and choose the more promising one to optimize via mutagenesis and screening. We used a previously developed single-strain microfluidic device with a variety of cell trap sizes and a concentration gradient (Miano et al., 2020) to characterize the behavior of both the designs for varying levels of anhydrotetracycline (aTc). The first implementation of the P2N2-Tet design did not lead to oscillations in any of the cell traps analyzed. Instead, this circuit only displayed single GFP peaks that quickly decayed to steady-state GFP levels, as shown in the representative time trace in Figure 4D (bottom). Furthermore, GFP peaks for this design were only seen in the three largest trap sizes, and the steady-state mean trap GFP fluorescence was proportional to the concentration of aTc in the media (Figures S3A and S3C). By contrast, the initial version of the P2N1-Tet design occasionally displayed clear oscillatory peaks (Figure 4C); however, oscillations were never seen in the largest trap size tested and only seen in 37.5% of the 32 cell traps analyzed for the next two smallest trap sizes.

To better understand the differences we saw experimentally between the two oscillator designs, we created a mathematical model consisting of delayed ordinary differential equations. In the model for the P2N1-Tet design, we saw that oscillatory behavior could be achieved for smaller values of the delay parameter than for the P2N2 design (Figures 4E and 4F). Specifically, when the delay term, τ, was set to one, the P2N2-Tet design displayed a single peak in TetR-GFP expression followed by a rapid decay to a steady-state value. On the other hand, we found that the P2N1 design could achieve oscillatory behavior even when the delay term was set to one (Figure 4E). Based on this, we hypothesized that the experimentally observed lack of oscillations for the P2N2-Tet design was due to insufficient delay in the negative feedback caused by TetR repression. We also looked at the effect that repressor cooperativity had on the propensity for oscillatory behavior in our model of the P2N2-Tet circuit. We found that for increased repressor cooperativity (i.e., hill coefficient of 2 versus 4), the P2N2 design could generate oscillations for smaller values of the delay parameter, τ (Figure S3B). This corresponds well with the results obtained from the two-strain oscillator study of Chen et al. as well as with the previous oscillator studies from our group demonstrating that LacI (higher hill coefficient than TetR) negative autoregulation can be a feature of robust oscillator circuit designs (Stricker et al., 2008).

In modeling the P2N1-Tet oscillator design, we also found that the existence of sustained oscillations was highly dependent on the maximum TetR expression rate. Specifically, if the TetR expression rate parameter was not sufficiently high, the model predicted oscillations that would quickly decay over time (Figure 4E). Based on these results, we hypothesized that we could optimize our initial implementation of the P2N1-Tet design to exhibit more regular oscillations by tuning the expression strength of TetR-GFP by directed mutagenesis followed by the screening of the resultant library with our multiplexed microfluidic device.

To create a mutant library where TetR expression strength is varied, we changed the RBS preceding TetR (highlighted in Figure 4A) to RBS sequences derived from the Anderson Lab RBS collection (Anderson et al., 2010) by SDM. The final library consisted of as many as 4,096 unique sequences. For the initial screening of this circuit library, we picked 48 unique colonies and screened them in batch culture using a 96-well plate in the presence and absence of 100 ng/mL aTc and tracked their GFP expression during growth (Figure 5A). For further screening in microfluidics, we selected 8 library members that spanned the range of GFP expression we saw in the well plate assay and loaded these strains on the multistrain microfluidic platform. Only 8 out of the 48 strains from the batch culture screen were chosen to culture in the microfluidic device because these strains spanned the range of GFP fluorescence levels we saw in the batch culture screen. When grown in the multistrain device, the majority of library strains exhibited one or two small peaks in TetR-GFP expression before decaying to relatively steady, intermediate levels of expression (Figure 5B).

The original P2N1-Tet strain and strain D1 were the only two screened strains that consistently had more than one GFP peak in the multistrain device. To quantify the differences between the damped oscillations shown by the original strain and strain D1, we fit replicate GFP traces for each strain with a decaying exponential function to determine the effective damping coefficient for each strain. Strain D1 had a smaller damping coefficient than the original strain, indicating the strain D1 was closer to displaying sustained oscillations in this device. In order to further study the behavior of strain D1 and compare it with the original P2N1-Tet strain, we grew strain D1 in the single-strain microfluidic device used to initially characterize the original P2N1-Tet strain.

When strain D1 was grown in the microfluidic chip with variable trap sizes, we found that it exhibited regular oscillations over long time periods in multiple trap sizes (Figures 5C and S4A; Video S3). Specifically, strain D1 was able to oscillate in larger trap sizes, had a larger amplitude, and oscillated in a much larger percentage of cell traps than the original P2N1-Tet strain (Figures 5C, 5D, S4A, and S4B). Moreover, we found that strain D1 had less variability in oscillatory period than the original strain, as shown in the peak-peak interval histogram in Figure 5E.

Additionally, we found that the characteristics of the oscillations for the D1 strain were unaffected by aTc concentrations ranging from 0 to 50 ng/mL, with no clear impact on period or amplitude (Figures S4B and S4D). Although this apparent insensitivity to aTc could be a result of aTc degradation during the experiment due to the molecule's photosensitivity, our previous experiment with the P2N2 design suggests that aTc is stable for at least 20 h in the microfluidic experiments, as we observed stable aTc-mediated TetR-GFP expression differences maintained for more than a day in that experiment (Figure S3D). Modeling results suggested that aTc would increase the DC offset of oscillations as well as extend the period of the P2N1-Tet design (Figure S4E). Thus, it is likely that the lack of aTc impact we saw was a result of the concentrations being too low compared

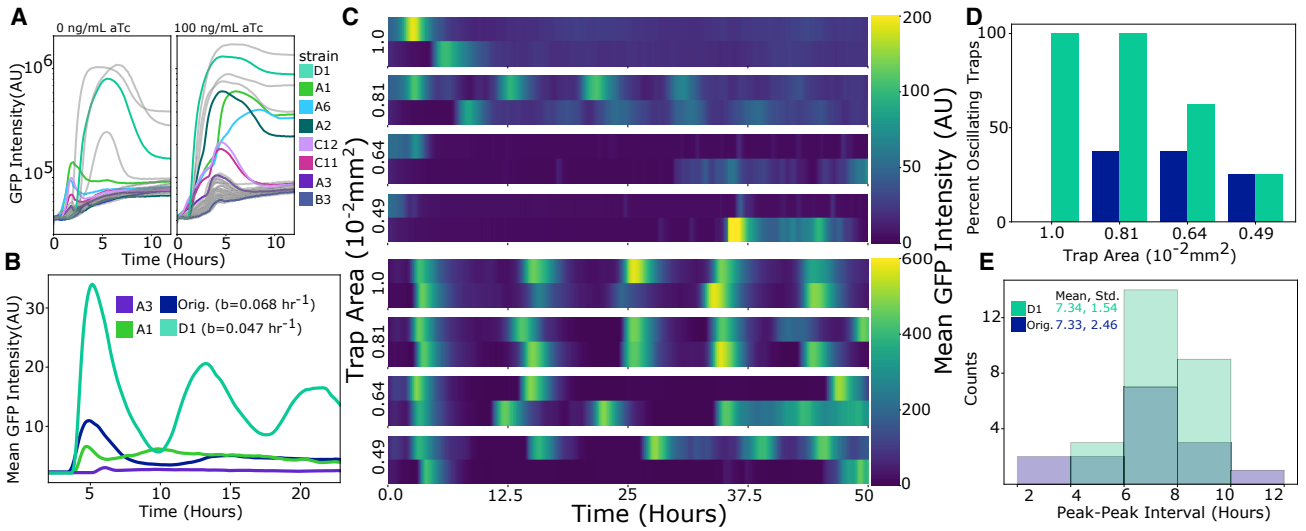

Figure 5. Optimizing a synchronized genetic oscillator via directed mutagenesis and screening

(A) A library of potential oscillator strains was created by randomizing the RBS in front of the *tetR-gfp* gene by SDM. All the strains were screened for differences in TetR-GFP expression in batch culture in the presence of 0 or 100 ng/mL aTc. The eight highlighted strains were selected for additional characterization and testing in the multistrain microfluidic platform.

(B) Representative TetR-GFP time traces for a subset of strains screened in the multistrain platform. Damping coefficients, b, were calculated for the original strain and strain D1 by fitting the GFP time traces with decaying exponential functions. The reported coefficient values represent the mean value for 4 replicate cell traps and 12 replicate cell traps for the original and D1 strains, respectively. Standard deviations for mean coefficient values were 0.0053 and 0.011 for the original and D1 strains, respectively.

(C) Heatmaps showing oscillatory dynamics for the original implementation of the synchronized oscillator (top) and oscillator library strain D1 (bottom) in cell traps of different sizes with 50 ng/mL aTc. Color scale is linear and represents mean trap GFP signal (AU).

(D) Comparison of the number of cell traps that exhibited oscillations for both strains. For each cell trap size, 16 unique cell traps were analyzed. Oscillatory behavior was defined as a given cell trap population showing 3 or more peaks in mean GFP fluorescence during a 50-h time window.

(E) Peak-peak interval histogram comparing the dynamics of the original strain to strain D1 in cell traps with an area of 0.81E−2 mm^2. Counts represent the number of peak-peak pairs observed across 16 cell traps for each strain.

with the very strong TetR expression. For instance, aTc concentrations of 100 ng/mL are often used for the full induction of TetR-repressible promoters in *E. coli* Mg1655 Z1, a strain with constitutive genomic production of TetR (Rodrigo et al., 2012). It is likely that the TetR-expression level is much higher in the P2N1-Tet circuit due to the LuxI-mediated positive feedback, relatively high plasmid copy number, and lack of negative autoregulation to prevent TetR levels from increasing rapidly before the AHL production is shutoff. Lastly, the period of the D1 oscillator was also able to be tuned by varying the flow rate, with reduced flow rate leading to more frequent oscillations (Figure S4C).

Although our experimental data strongly suggest that the RBS in the D1 oscillator strain led to stronger TetR-GFP expression levels than those in the original P2N1 oscillator strain, we again looked at translation rates predicted by the RBS calculator. We found that the RBS calculator results did not correlate well with our experimental results, with the calculator predicting a translation rate of 9,438 for the original RBS and 1,658 for the D1 RBS. As we did for the RBS sequences from the lysis circuit library, we cloned these RBS sequences in front of a constitutive promoter on a low-copy plasmid driving sfGFP expression. In this circuit, the D1 RBS had about 4-fold more GFP expression than the original P2N1 RBS. In this context, the RBS calculator again predicted a stronger expression for the original RBS (translation rate of 6,614) than for the D1 RBS (3,728) in direct contrast to the experimental results (Figure S5B). Together, these results further highlight the utility of screening genetic circuit variants for desired behavior even when rational design tools exist.

DISCUSSION

Tuning genetic circuits by screening variant libraries for desired phenotypes has long been fundamental to synthetic biology design. However, the mass-screening of dynamic phenotypes has remained a persistent challenge, and our ability to generate genotypic diversity far exceeds our ability to screen complex phenotypes (Schaerli and Isalan, 2013). Despite limited means for dynamic phenotype screening, canonical gene circuit motifs, including oscillators, logic gates, and feedback controllers, have been increasingly deployed in time-dependent applications spanning metabolic engineering to therapeutic delivery (Aoki et al., 2019; Din et al., 2016; Doong et al., 2018; Moser et al., 2018; Urrios et al., 2018). Multiplexed microfluidics, such as ours, can aid in the development of circuits like these for both academic research and real-world applications.

For bacteria, it is well documented that the growth state of a growing culture has a significant impact on gene expression (Caglar et al., 2017; Scott et al., 2010; Takahashi et al., 2015). Thus, to reliably characterize and evaluate complex circuit dynamics, the cellular growth environment should be as constant as possible. In this article, we further demonstrate the

importance of continuous culture screening, specifically in the context of dynamic gene circuits like oscillators. In screening the SLC library, we saw that the presence of a lysis event in the batch culture screen generally correlated with a propensity for robust oscillations in continuous culture, but continuous culture was necessary to confirm and detect sustained oscillations for any library members. On the other hand, batch screening of the TetR-GFP synchronized oscillator provided little evidence regarding which strains were more likely to oscillate in microfluidic culture but did facilitate the selection of strains with varying TetR expressions for further testing in microfluidics. One likely reason why oscillations were not seen in batch culture for the TetR synchronized oscillator is that the oscillatory period of the circuit that was seen in microfluidics (around 10 h) is considerably longer than the time the cellular population remained in exponential phase (around 3–4 h) during batch culture. Although our results show that batch culture can offer some insights into the design of oscillator circuits, in this context, batch culture is most useful as a means to cull uninteresting variations in dynamic gene circuit libraries. Ultimately, the microfluidic approach is necessary for fully characterizing the dynamic phenotypes.

Microfluidic culturing systems have served as useful tools for approximating complex real-world environments in the past, simulating environments spanning soil to human organs (Rusconi et al., 2014; Zhang et al., 2018). Although not a perfect recreation of these complex environments, tuning environmental and time-dependent parameters with microfluidics serves an important role in prototyping and scaling up gene circuits. This work shows how environment, specifically population size, can significantly impact the circuit dynamics, with the TetR synchronized oscillator behaving differently when grown in different cell trap geometries. Understanding how circuit dynamics change, or are resistant to change, as trap size varies can be critical to predicting how a circuit might behave when deployed in a real-world, nonmicrofluidic environment.

One challenge in engineering *population-level* behaviors is that they are resistant to screening with sufficiently high throughput to interrogate the large libraries typically needed for directed evolution where complex sequences such as those encoding proteins are targeted to improve strain performance. Although some of the novel, pooled-library approaches for screening complex phenotypes described earlier achieve orders of magnitude greater throughput than what we present here, there is no clear path forward to adapt those approaches to situations where desired phenotypes for a given strain are seen only in large population sizes or when the strain is spatially isolated from all other library members. Thus, in the future, we could envision workflows where key single-cell indicator phenotypes that are suggestive of population-level phenotypes are first screened for using high-throughput pooled library techniques and then a subset of interesting variants is screened at the population level using an arrayed, continuous culture platform similar to the one we present here. In the future, the throughput of our device could potentially be increased to accommodate on the order of 1,000 unique strains as indicated by our groups' previous work on using large bacterial libraries for biosensing (Graham et al., 2020).

STAR★METHODS

Detailed methods are provided in the online version of this paper and include the following:

- KEY RESOURCES TABLE
- RESOURCE AVAILABILITY
  - Lead contact
  - Materials availability
  - Data and code availability
- EXPERIMENTAL MODEL AND SUBJECT DETAILS
  - Escherichia coli strain MG1655
- METHOD DETAILS
  - Cloning and library creation for SLC strains
  - Cloning and library creation for TetR synchronized oscillator strains
  - Microfluidic device development and fabrication
  - Multi-strain microfluidic experimental protocol
  - AHL induction protocol in SLC microfluidic experiments
  - Live-cell imaging and data extraction for SLC library experiments
  - Single strain microfluidic device loading and bonding
  - Generation of lysis dose-response curves
  - Calculation of damping coefficients
  - Peak detection for comparison of P2N1-Tet strains
  - Data analysis of multi-strain microfluidic transmitted-light image stacks
  - Analysis of single strain microfluidic data
  - Theoretical RBS translation rate prediction with RBS Calculator 2.0
  - Experimental characterization of selected RBS sequences in constitutive GFP expressing circuit
  - Deterministic modeling of Synchronized Lysis Circuit dynamics
  - Deterministic modeling of tetR-GFP synchronized oscillator dynamics
- QUANTIFICATION AND STATISTICAL ANALYSIS

SUPPLEMENTAL INFORMATION

Supplemental information can be found online at https://doi.org/10.1016/j.cels.2022.02.005.

ACKNOWLEDGMENTS

This work was supported by the National Institute of General Medical Sciences of the National Institutes of Health (grant no. R01GM069811). A.L. was supported by the National Science Foundation Graduate Research Fellowship Program under grant no. DGE-2038238. Any opinions, findings, and conclusions or recommendations expressed in this material are those of the authors and do not necessarily reflect the views of the National Science Foundation. The authors thank Arianna Miano for providing the device for single-strain microfluidic experiments, Elizabeth Stasiowski and Richard O'Laughlin for input on the design of the multistrain microfluidic device, Jaquelin Dezha Peralta for assistance with microfluidic fabrication, and Shalni Kumar for critical reading of the manuscript.

AUTHOR CONTRIBUTIONS

Conceptualization, A.L., N.C., and J.H.; investigation, A.L. and N.C.; writing and visualization, A.L., N.C., and J.H.

DECLARATION OF INTERESTS

J.H. is a founder of GenCirq and Quantitative Biosciences, which focus on cancer therapeutics and agricultural synthetic biology, respectively. J.H. is a shareholder in both these companies and is on their scientific advisory boards. N.C. is currently employed with Quantitative Biosciences.

Received: June 25, 2021
Revised: November 15, 2021
Accepted: February 17, 2022
Published: March 22, 2022

REFERENCES

Alexander, D.L., Lilly, J., Hernandez, J., Romsdahl, J., Troll, C.J., and Camps, M. (2014). Random mutagenesis by error-prone pol plasmid replication in *Escherichia coli*. In Directed Evolution Library Creation (Springer), pp. 31–44.

Anderson, J., Dueber, J.E., Leguia, M., Wu, G.C., Goler, J.A., Arkin, A.P., and Keasling, J.D. (2010). BglBricks: a flexible standard for biological part assembly. J. Biol. Eng. *4*, 1–12.

Aoki, S.K., Lillacci, G., Gupta, A., Baumschlager, A., Schweingruber, D., and Khammash, M. (2019). A universal biomolecular integral feedback controller for robust perfect adaptation. Nature *570*, 533–537.

Baumgart, L., Mather, W., and Hasty, J. (2017). Synchronized DNA cycling across a bacterial population. Nat. Genet. *49*, 1282–1285.

Bernhardt, T.G., Roof, W.D., and Young, R. (2000). Genetic evidence that the bacteriophage φX174 lysis protein inhibits cell wall synthesis. Proc. Natl. Acad. Sci. USA *97*, 4297–4302.

Bull, A.T. (2010). The renaissance of continuous culture in the post-genomics age. J. Ind. Microbiol. Biotechnol. *37*, 993–1021.

Caglar, M.U., Houser, J.R., Barnhart, C.S., Boutz, D.R., Carroll, S.M., Dasgupta, A., Lenoir, W.F., Smith, B.L., Sridhara, V., Sydykova, D.K., et al. (2017). The *E. coli* molecular phenotype under different growth conditions. Sci. Rep. *7*, 1–15.

Camsund, D., Lawson, M.J., Larsson, J., Jones, D., Zikrin, S., Fange, D., and Elf, J. (2020). Time-resolved imaging-based CRISPRi screening. Nat. Methods *17*, 86–92.

Chen, Y., Kim, J.K., Hirning, A.J., Josić, K., and Bennett, M.R. (2015). Synthetic biology. Emergent genetic oscillations in a synthetic microbial consortium. Science *349*, 986–989.

Danino, T., Mondragón-Palomino, O., Tsimring, L., and Hasty, J. (2010). A synchronized quorum of genetic clocks. Nature *463*, 326–330.

Del Vecchio, D. (2015). Modularity, context-dependence, and insulation in engineered biological circuits. Trends Biotechnol. *33*, 111–119.

Din, M.O., Danino, T., Prindle, A., Skalak, M., Selimkhanov, J., Allen, K., Julio, E., Atolia, E., Tsimring, L.S., Bhatia, S.N., and Hasty, J. (2016). Synchronized cycles of bacterial lysis for *in vivo* delivery. Nature *536*, 81–85.

Doong, S.J., Gupta, A., and Prather, K.L.J. (2018). Layered dynamic regulation for improving metabolic pathway productivity in Escherichia coli. Proc. Natl. Acad. Sci. USA *115*, 2964–2969.

Emanuel, G., Moffitt, J.R., and Zhuang, X. (2017). High-throughput, image-based screening of pooled genetic-variant libraries. Nat. Methods *14*, 1159–1162.

Espah Borujeni, A., Channarasappa, A.S., and Salis, H.M. (2014). Translation rate is controlled by coupled trade-offs between site accessibility, selective RNA unfolding and sliding at upstream standby sites. Nucleic Acids Res. *42*, 2646–2659.

Esvelt, K.M., Carlson, J.C., and Liu, D.R. (2011). A system for the continuous directed evolution of biomolecules. Nature *472*, 499–503.

Ferrell, J.E., Jr., and Ha, S.H. (2014). Ultrasensitivity part III: cascades, bistable switches, and oscillators. Trends Biochem. Sci. *39*, 612–618.

Ferry, M.S., Razinkov, I.A., and Hasty, J. (2011). Chapter fourteen-microfluidics for synthetic biology: from design to execution. In Synthetic Biology, Part A, C. Voigt, ed. (Academic Press), pp. 295–372. https://doi.org/10.1016/B978-0-12-385075-1.00014-7.

Gallagher, R.R., Li, Z., Lewis, A.O., and Isaacs, F.J. (2014). Rapid editing and evolution of bacterial genomes using libraries of synthetic DNA. Nat. Protoc. *9*, 2301–2316.

Gibson, D.G., Young, L., Chuang, R.Y., Venter, J.C., Hutchison, C.A., and Smith, H.O. (2009). Enzymatic assembly of DNA molecules up to several hundred kilobases. Nat. Methods *6*, 343–345.

Graham, G., Csicsery, N., Stasiowski, E., Thouvenin, G., Mather, W.H., Ferry, M., Cookson, S., and Hasty, J. (2020). Genome-scale transcriptional dynamics and environmental biosensing. Proc. Natl. Acad. Sci. USA *117*, 3301–3306.

Grandel, N.E., Reyes Gamas, K.R., and Bennett, M.R. (2021). Control of synthetic microbial consortia in time, space, and composition. Trends Microbiol. *29*, 1095–1105.

Halperin, S.O., Tou, C.J., Wong, E.B., Modavi, C., Schaffer, D.V., and Dueber, J.E. (2018). CRISPR-guided DNA polymerases enable diversification of all nucleotides in a tunable window. Nature *560*, 248–252.

Haseltine, E.L., and Arnold, F.H. (2007). Synthetic gene circuits: design with directed evolution. Annu. Rev. Biophys. Biomol. Struct. *36*, 1–19.

Hasty, J. (2002). Design then mutate. Proc. Natl. Acad. Sci. *99*, 16516–16518.

Jain, P.C., and Varadarajan, R. (2014). A rapid, efficient, and economical inverse polymerase chain reaction-based method for generating a site saturation mutant library. Anal. Biochem. *449*, 90–98.

Karamasioti, E., Lormeau, C., and Stelling, J. (2017). Computational design of biological circuits: putting parts into context. Mol. Syst. Des. Eng. *2*, 410–421.

Lawson, M.J., Camsund, D., Larsson, J., Baltekin, Ö., Fange, D., and Elf, J. (2017). *In situ* genotyping of a pooled strain library after characterizing complex phenotypes. Mol. Syst. Biol. *13*, 947.

Lepzelter, D., Feng, H., and Wang, J. (2010). Oscillation, cooperativity, and intermediates in the self-repressing gene. Chem. Phys. Lett. *490*, 216–220.

Liu, H., and Naismith, J.H. (2008). An efficient one-step site-directed deletion, insertion, single and multiple-site plasmid mutagenesis protocol. BMC Biotechnol. *8*, 91.

Luro, S., Potvin-Trottier, L., Okumus, B., and Paulsson, J. (2020). Isolating live cells after high-throughput, long-term, time-lapse microscopy. Nat. Methods *17*, 93–100.

Miano, A., Liao, M.J., and Hasty, J. (2020). Inducible cell-to-cell signaling for tunable dynamics in microbial communities. Nat. Commun. *11*, 1193.

Moser, F., Espah Borujeni, A., Ghodasara, A.N., Cameron, E., Park, Y., and Voigt, C.A. (2018). Dynamic control of endogenous metabolism with combinatorial logic circuits. Mol. Syst. Biol. *14*, e8605.

Napolitano, M.G., Landon, M., Gregg, C.J., Lajoie, M.J., Govindarajan, L., Mosberg, J.A., Kuznetsov, G., Goodman, D.B., Vargas-Rodriguez, O., Isaacs, F.J., et al. (2016). Emergent rules for codon choice elucidated by editing rare arginine codons in Escherichia coli. Proc. Natl. Acad. Sci. USA *113*, E5588–E5597.

Nielsen, A.A., Der, B.S., Shin, J., Vaidyanathan, P., Paralanov, V., Strychalski, E.A., Ross, D., Densmore, D., and Voigt, C.A. (2016). Genetic circuit design automation. Science *352*, aac7341.

Orth, P., Schnappinger, D., Hillen, W., Saenger, W., and Hinrichs, W. (2000). Structural basis of gene regulation by the tetracycline inducible Tet repressor-operator system. Nat. Struct. Biol. *7*, 215–219.

Prindle, A., Samayoa, P., Razinkov, I., Danino, T., Tsimring, L.S., and Hasty, J. (2011). A sensing array of radically coupled genetic 'biopixels'. Nature *481*, 39–44.

Reis, A.C., and Salis, H.M. (2020). An automated model test system for systematic development and improvement of gene expression models. ACS Synth. Biol. *9*, 3145–3156.

Rodrigo, G., Landrain, T.E., and Jaramillo, A. (2012). De novo automated design of small RNA circuits for engineering synthetic riboregulation in living cells. Proc. Natl. Acad. Sci. USA *109*, 15271–15276.

Rusconi, R., Garren, M., and Stocker, R. (2014). Microfluidics expanding the frontiers of microbial ecology. Annu. Rev. Biophys. *43*, 65–91.

Rutkauskas, D., Zhan, H., Matthews, K.S., Pavone, F.S., and Vanzi, F. (2009). Tetramer opening in LacI-mediated DNA looping. Proc. Natl. Acad. Sci. USA *106*, 16627–16632.

Salis, H.M., Mirsky, E.A., and Voigt, C.A. (2009). Automated design of synthetic ribosome binding sites to control protein expression. Nat. Biotechnol. *27*, 946–950.

Schaerli, Y., and Isalan, M. (2013). Building synthetic gene circuits from combinatorial libraries: screening and selection strategies. Mol. Biosyst. *9*, 1559–1567.

Scott, M., Gunderson, C.W., Mateescu, E.M., Zhang, Z., and Hwa, T. (2010). Interdependence of cell growth and gene expression: origins and consequences. Science *330*, 1099–1102.

Scott, S.R., Din, M.O., Bittihn, P., Xiong, L., Tsimring, L.S., and Hasty, J. (2017). A stabilized microbial ecosystem of self-limiting bacteria using synthetic quorum-regulated lysis. Nat. Microbiol. *2*, 17083.

Sepich-Poore, G.D., Zitvogel, L., Straussman, R., Hasty, J., Wargo, J.A., and Knight, R. (2021). The microbiome and human cancer. Science *371*, eabc4552.

Song, H., Payne, S., Tan, C., and You, L. (2011). Programming microbial population dynamics by engineered cell–cell communication. Biotechnol. J. *6*, 837–849.

Stricker, J., Cookson, S., Bennett, M.R., Mather, W.H., Tsimring, L.S., and Hasty, J. (2008). A fast, robust and tunable synthetic gene oscillator. Nature *456*, 516–519.

Takahashi, C.N., Miller, A.W., Ekness, F., Dunham, M.J., and Klavins, E. (2015). A low cost, customizable turbidostat for use in synthetic circuit characterization. ACS Synth. Biol. *4*, 32–38.

Urrios, A., Gonzalez-Flo, E., Canadell, D., de Nadal, E., Macia, J., and Posas, F. (2018). Plug-and-play multicellular circuits with time-dependent dynamic responses. ACS Synth. Biol. *7*, 1095–1104.

Weber, E., Engler, C., Gruetzner, R., Werner, S., and Marillonnet, S. (2011). A modular cloning system for standardized assembly of multigene constructs. PLoS One *6*, e16765.

Wu, M.R., Jusiak, B., and Lu, T.K. (2019). Engineering advanced cancer therapies with synthetic biology. Nat. Rev. Cancer *19*, 187–195.

Yokobayashi, Y., Weiss, R., and Arnold, F.H. (2002). Directed evolution of a genetic circuit. Proc. Natl. Acad. Sci. USA *99*, 16587–16591.

Zeng, F., Zhang, S., Hao, Z., Duan, S., Meng, Y., Li, P., Dong, J., and Lin, Y. (2018). Efficient strategy for introducing large and multiple changes in plasmid DNA. Sci. Rep. *8*, 1714.

Zhang, B., Korolj, A., Lai, B.F.L., and Radisic, M. (2018). Advances in organ-on-a-chip engineering. Nat. Rev. Mater. *3*, 257–278.

Zhou, S., Gravekamp, C., Bermudes, D., and Liu, K. (2018). Tumour-targeting bacteria engineered to fight cancer. Nat. Rev. Cancer *18*, 727–743.

STAR★METHODS

KEY RESOURCES TABLE

REAGENT or RESOURCE	SOURCE	IDENTIFIER
Bacterial and virus strains		
Escherichia coli strain MG1655	ATCC	NCBI: txid511145
Chemicals, peptides, and recombinant proteins		
N-(β-Ketocaproyl)-L-homoserine lactone (*N*-(3-Oxohexanoyl)-L-homoserine lactone)	Sigma-Aldrich	Cat#: K3007
Anhydrotetracycline (hydrochloride)	Cayman Chemical Company	Cat#:13803-65-1
Experimental models: Organisms/strains		
Escherichia coli strain MG1655		NCBI: txid511145
Oligonucleotides		
5′CATTAAAGAGNNNNNAGGTACCATGATGGTAC3′	Integrated DNA Technologies (IDT)	N/A
5′AATTCTCTCTATCACTGATAG3′	Integrated DNA Technologies (IDT)	N/A
5′NNGANNNACTAGATGTCTAGATTAGATAAAAGTAAAG3′	Integrated DNA Technologies (IDT)	N/A
5′NTCTTTCTCTAGAATTCGACTATAACAAACCATTTTC3′	Integrated DNA Technologies (IDT)	N/A
Recombinant DNA		
pSpSLC Plasmid (and associated library plasmids)	Made in Lab	N/A
pTetSO1 Plasmid	Made in Lab	N/A
pTetSO2 Plasmid (and associated library plasmids)	Made in Lab	N/A
pTetSO3 Plasmid	Made in Lab	N/A
Software and algorithms		
MATLAB Version 2017B	MathWorks Academic License	N/A
Python 3	https://www.python.org/downloads/	N/A
RBS Calculator version 2.0	https://salislab.net/software/predict_rbs_calculator	N/A
ImageJ	https://imagej.net/software/imagej/	N/A
Other		
Labcyte Echo Series 550 Liquid Handler	Labcyte (Now owned by Beckman Coulter)	Product No:001-16079

RESOURCE AVAILABILITY

Lead contact

Further information and requests for resources should be directed to and will be fulfilled by the lead contact, Dr. Jeff Hasty (jhasty@eng.ucsd.edu).

Materials availability

Plasmids generated in this study are available from the lead contact upon request.

Data and code availability

- All data reported in this paper will be shared by the lead contact upon request.
- This paper does not report original code.
- Any additional information required to reanalyze the data reported in this paper is available from the lead contact upon request.

EXPERIMENTAL MODEL AND SUBJECT DETAILS

Escherichia coli strain MG1655

Throughout this work *E. coli* MG1665 was grown in aerobic conditions at 37 degrees Celsius in the standard Lennox formulation of Luria Bertani Broth (LB) with the appropriate antibiotics for plasmid maintenance.

METHOD DETAILS

Cloning and library creation for SLC strains

The original version of the single-plasmid synchronized lysis circuit (pSpSLC_0) was created by Gibson Assembly using PCR-amplified DNA sequences obtained from previously existing lysis circuit plasmids developed in our lab. The plasmid sequence was confirmed with Sanger sequencing (Eton Bioscience, San Diego, CA). To generate a mutant library of the pSpSLC oscillator plasmid, 5 base pairs in the Shine-Dalgarno sequence of the ribosome binding site (located 7 to 12 base pairs upstream of the start codon of the lysis protein, E) were randomized by site directed mutagenesis. The original sequence at this position was: GAGAA. First, the entire plasmid was PCR amplified with the following degenerate primers where N indicates any base: 5′ CATTAAAGAGNNNNNAGG TACCATGATGGTAC 3′ and 5′ AATTCTCTCTATCACTGATAG 3′. The PCR reaction mix was incubated with DPNI at 37C for 30 minutes to digest template plasmid and then the 4.7 kb PCR product was run on an agarose gel and extracted using a QIAquick Gel Extraction Kit (QIAGEN). 1μL of the gel extracted PCR product was mixed with 0.5μL T4 ligase buffer, 0.5μL T4 PNK, and 3μL of DNase-free water and incubated at 37C. Next, 0.5μL T4 ligase buffer, 0.5μL T4 DNA ligase, and 4μL were added to the reaction mixture and the mixture was incubated at room temperature overnight. The following day, 50μL of chemically competent MG1655 E. coli cells were transformed with 3μL of the reaction mix and plated on an LB agar plate containing 0.2% glucose and spectinomycin. 24 colonies from the agar plate were randomly selected for mutant screening and grown up for 16 hours in LB media with 0.2% glucose and spectinomycin prior to use in experiments.

Cloning and library creation for TetR synchronized oscillator strains

Plasmids pTetSO1, pTetSO2, and pTetSO3 were created by Gibson Assembly using PCR-amplified DNA sequences obtained from previously existing plasmids created in our lab. Plasmid sequences were confirmed with Sanger sequencing (Eton Bioscience, San Diego, CA). To generate a mutant library of the two plasmid P2N1-Tet synchronized oscillator design, the RBS preceding TetR-GFP on the plasmid pTetSO2 was randomized to RBS sequences derived from an RBS library created by Professor Christopher Anderson (Anderson et al., 2010). Specifically, the entire plasmid was PCR amplified using Q5 DNA Polymerase with the following degenerate primers where N indicates any base: 5′ NNGANNNACTAGATGTCTAGATTAGATAAAAGTAAAG 3′ and 5′ NTCTTTCTCTAGAATTC GACTATAACAAACCATTTTC3′. Degenerate primers were ordered from Integrated DNA Technologies (IDT). A blunt-end ligation was performed to re-circularize the plasmid before co-transformation with plasmid pTetSO1 into MG1655 *E. coli* competent cells. The transformation was plated on LB agar containing chloramphenicol and spectinomycin and 48 colonies from the agar plate were randomly selected for mutant screening.

Microfluidic device development and fabrication

Our group has previously described the microfabrication techniques used to pattern SU-8 photoresist onto a silicon wafer to create the mold for our device (Ferry et al., 2011). A poly-dimethylsiloxane (PDMS) device was made from the wafer by mixing 77 grams of Sylgard 184 and pouring it on the wafer centered on a level 5''x5'' glass plate surrounded with an aluminum foil seal. The degassed wafer and PDMS was cured on a flat surface for one hour at 95°C.

Multi-strain microfluidic experimental protocol

For multi-strain microfluidic experiments, cells were grown overnight on LB+antibiotic media. Lysis oscillator strains were grown on LB supplemented with 0.2% glucose to suppress expression of the pLux promoter driving lysis. 45 μL of each cultured strain were transferred to its own well in a 384 Echo compatible plate for direct transfer onto microfluidic devices. A PDMS device cleaned with 70% Ethanol and adhesive tape was aligned to a custom fixture compatible with the Labcyte Echo. Both the fixture and a clean 4''x3'' glass slide sonicated with 2% Helmanex III were exposed to oxygen plasma. 2.5 nL of each strain were deposited from the 384 Echo compatible plate directly onto each PDMS device. The device and glass slide were bonded together and cured at 37°C for two hours. Before setting up a microfluidic experiment, the device was placed in a vacuum for a minimum of 20 minutes. The device was then mounted onto the custom optical enclosure. The inlet port was connected to a 50 mL syringe and tygon tubing with LB media with antibiotic (spectinomycin for SLC oscillator strains, chloramphenicol and spectinomycin for tetR-GFP synchronized oscillator strains), and 0.075% Tween-20. The waste port was connected to tygon tubing and a 1L waste bottle. The height difference between the inlet and outlet was 20'' corresponding to a flow rate of approximately 1 mL/hr. Tween-20 was used in the media as a surfactant to reduce clogging and therefore increase the longevity of microfluidic experiments. Tween-20 has been used by our group in many experiments without an adverse effect on *E. coli* (Ferry et al., 2011, Prindle et al., 2012). Microfludic experiments were performed on a custom optical enclosure or on a Nikon TE2000-U epifluorescent inverted microscope (Nikon Instruments Inc., Tokyo, Japan). Cells were grown on the device on LB media with the appropriate antibiotics, and 0.075% Tween-20 until traps were filled to confluence. Extracted fluorescence time series were normalized to remove device background fluorescence and strain background fluorescence.

AHL induction protocol in SLC microfluidic experiments

For AHL inductions, LB with the predetermined AHL concentration was mixed and pipetted into the source media syringe. For periods where the same AHL concentration was left on the device for over 24 hours, the media was pipetted out of the syringe and replaced every 12 hours.

Live-cell imaging and data extraction for SLC library experiments

Microfluidic devices were imaged in a custom optical enclosure continuously every ten minutes in both the transmitted light and GFP fluorescence channels with a 1 second and 60 second exposure respectively. The custom optical enclosure uses an SBIG STX-16803 CCD Camera with a custom lens stack assembly containing the Semrock FF01-466/40-32-D-EB and FF02-520/28-50-D-EB excitation and emission filters, respectively. The enclosure has green and blue LED spotlight sources obtained from ProPhotonix for transmitted light and fluorescence light sources, respectively. The optical resolution of the enclosure is 36 μm. The enclosure was temperature controlled to 37°C.

Images were synced from the enclosure to a server via WiFi for further data processing. Custom software produced flat-field-corrected images in both channels in real-time to remove optical vignetting using the following equation:

$$C = m * \frac{R - D}{F' - D'} \quad \text{(Equation 1)}$$

where R is the raw image to be flat-field corrected, D is the dark-current image for that device, taken at the same exposure settings as R, F' is a raw image taken by the camera with no device present, D' is the dark-current image taken at same exposure as F', m is the mean value for all values in the array $(F' - D')$, and C is the resulting corrected image.

Flat-field corrected images were then processed in ImageJ, where a custom "Region Of Interest" or ROI manager was used to extract fluorescence, transmitted light, and background values.

Data was initially processed by subtracting the local background signal, in order to eliminate any local or regional fluctuations that are of an additive (or, analogously, subtractive) nature. The result of this background correction was to produce a vector $\overrightarrow{x_t}$ representing the background-corrected fluorescent signals of all cell traps at time t:

$$x_{(t,s_i)} = x^{trap}_{(t,s_i)} - x^{background}_{(t,s_i)} \quad \text{(Equation 2)}$$

where t refers to the current time point, s_i refers to the strain in cell trap i, $x^{trap_{(t,s_i)}}$ is the flat-field corrected fluorescent signal from the *trap* of position i at time t, and $x^{background}_{(t,s_i)}$ refers to the flat-field corrected local background fluorescent signal at position i at time t.

Once extracted, period and peak analysis was performed on fluorescence traces using the find_peaks function in the scipy signal processing toolbox, filtering for peaks with a minimum prominence of 10 (arbitrary fluorescence units).

Single strain microfluidic device loading and bonding

For the single-strain microfluidic experiments, a previously developed PDMS device with variable cell trap sizes and a concentration gradient generator was used (Miano et al., 2020). Prior to cell loading, the device was placed in a vacuum chamber for 30 minutes. During this period, 1mL of an overnight culture of the engineered strain was spun down and concentrated in 10μL of LB media with 0.075% tween. Immediately following removal from the chamber, the cell suspension was pipetted to cover the outlet of the device and sterile LB media + 0.075% tween was pippetted to cover the two inlet ports. After media and cells were pulled into the microfluidic chip by the vacuum and the cell traps had filled with cells, two inlet syringes with fluidic tubing attached were connected to the inlet ports of the device. Similarly, an outlet syringe with tubing was connected to the outlet port of the device. All of the cell traps had the same width (100μm) and height (1.2μm) and ranged in length from 40 to 100μm. Media flow was maintained across the device by maintaining the source syringes 5-10 inches above the outlet syringe fluid height. For experiments using anhydrotetracycline (aTc), one inlet syringe was prepared with a concentration of 50ng/mL aTc in LB while the other syringe was prepared with 0ng/mL aTc leading to a gradient of 8 different aTc concentrations across the device.

Generation of lysis dose-response curves

To generate the lysis dose-response curves shown in Figure 3, 200μL cultures of the strains containing the plasmid pAHL_Lyse were started by seeding cells from a saturated culture at a 1:100 ratio in LB media. The cultures were grown at 37C and optical density was monitored every five minutes using a TECAN microplate reader with orbital shaking. Once the cultures reached early exponential phase (OD 0.2-0.3), the well plate was quickly removed them the microplate reader and each culture well was spiked with 2μL of a 100X AHL stock to achieve the desired final concentration. The well plate was then re-inserted into the microplate reader and the cultures were grown for 12 hours.

To calculate a lysis magnitude value from each condition, the growth curve for that condition was examined for an inflection point where the derivative of the culture OD with respect to time changed from positive to negative. Then, lysis magnitude was calculated as L/G, where G is the positive change in OD from the initial time point to the inflection point and L is the negative change in OD from the inflection point to the time point at which OD was lowest following the inflection point (Figure S2B). A dose response curve was generated with the lysis magnitude vs. AHL concentration data by fitting the data to the Hill Equation.

Calculation of damping coefficients

To calculate the damping coefficients (b) presented in Figure 5B for the original P2N1-Tet strain and strain D1 in the multistrain microfluidic device, the following equation was fit to the mean GFP intensity for a given cell trap using the curve_fit function in the SciPy python library: $GFP(t) = Ae^{(-b*t)}$.

Peak detection for comparison of P2N1-Tet strains

To compare the percentage of traps with oscillations between the original P2N1-Tet strain and strain D1 (Figure 4D), 50 hours of single strain microfluidic data for both strains was analyzed for peaks using the find_peaks function in the SciPy python library. To account for the differences in amplitude between the two oscillators, the height threshold in the peak finding script was changed for analysis of the two strains.

Data analysis of multi-strain microfluidic transmitted-light image stacks

To calculate the normalized cell density vs. time plots shown in Figure 3 using 10x transmitted light (TL) microscope images, the following protocol was used. First, the mean TL pixel value for each trap (TL_{trap}) was extracted in ImageJ along with the mean pixel value for a selection of equal size on a part of the chip containing no cells (TL_{BG}). To obtain an approximate cell density from these two measurements, the following formula was used: $CellDensity = Log\left(1 + \frac{TL_{BG}}{TL_{trap}}\right)$. Lastly, for each trap the approximate cell density was normalized as: $NormalizedCD = \frac{CD - min(CD)}{max(CD) - min(CD)}$

Analysis of single strain microfluidic data

To analyze the 10x image stacks obtained from time-lapse microscopy experiments with the TetR-GFP synchronized oscillator strains, the mean GFP pixel intensity from each image was extracted using imageJ for each trap size and inducer concentration. The data shown in Figures S4A and S4B represent the mean, background-subtracted GFP data for two separate microfluidic experiments. To calculate the average oscillatory period for the D1 oscillator for different conditions (Figure S4C), cell traps were chosen that had at least two distinct peaks in mean GFP expression for each flow rate and trap size combination. The period for each cell trap that was included in the data analysis was calculated as the mean time elapsed between each peak divided by the number of GFP peaks. The bar plot in Figure S4C was created by taking the mean period for each flow rate and trap combination and the error bars represent the standard deviation among analyzed cell traps.

Theoretical RBS translation rate prediction with RBS Calculator 2.0

To estimate the relative translation initiation rates for specific RBS sequences from the different mutant libraries (Figures S5A and S5B), Version 2.1 of the RBS calculator developed by Salis et al. was used (https://salislab.net/software/predict_rbs_calculator) (Reis and Salis, 2020). Specifically, the full mRNA sequence (including the 5′ non-coding region and the downstream coding sequence) were input into the RBS Calculator's prediction function. The values reported in the results and shown in the bar charts of Figures S5A and S5B represent the predicted translation initiation rate (AU) for the start codon of the relevant gene.

Experimental characterization of selected RBS sequences in constitutive GFP expressing circuit

To experimentally determine the relative expression strength for specific RBS sequences from the different mutant libraries (Figures S5A and S5B), these RBS sequences were cloned in front of a GFP gene driven by a constitutively active promoter. After verifying the resultant strains by sequencing, each strain was grown in LB media in a 96-well plate and GFP was monitored over time using a TECAN microplate reader. The values shown in the bar chart of Figures S5A and S5B represent the mean GFP/OD value (n=5) for each strain when the strain was in an exponential growth phase at an OD of 0.4.

Deterministic modeling of Synchronized Lysis Circuit dynamics

For all modeling of the SLC, we used a modified version of a previously published deterministic model of SLC dynamics (Scott et al., 2017). This simple model consists of two differential equations, one that describes the production and dilution of the quorum sensing molecule AHL (Equation 3) and one that describes cell growth and lysis-induced cell death (Equation 4). We added an additional ODE to this model to directly account for AHL-induced GFP production (Equation 5). To model the effect of exogeneous AHL on circuit dynamics (Figure S2A), we modified Equation 3 so that the value of AHL at any given time-point ($AHL(t)$) was not allowed to decrease below some set point AHL_{min}. We did not explicitly include a delay term in the SLC model that accounts for delays in transcription and translation of LuxI relative to the rapid binding of the AHL-LuxR complex to the pLux promoter. This choice was made because the cellular growth and lysis dynamics accounted for by the model occur on a much slower time scale than delays in gene expression making inclusion of a delay term in the hill function for LuxR-AHL binding unnecessary to predict circuit dynamics. All model results were obtained in MATLAB using the ode45 function. The following parameters were used in the SLC model simulations except where noted: $K = 2, D_{lysis} = 5, A_0 = 0.4, A_{max} = 8, AHL_{th} = 1, m = 4, A_{deg} = 1, G_{max} = 8, G_{deg} = 1, GFP_{th} = 3$

$$\frac{dAHL}{dt} = (A_0 + A_{max}F_A(AHL))n(t) - A_{deg}AHL(t) \quad \text{(Equation 3)}$$

$$\frac{dn}{dt} = Kn(t) - F_A(AHL)D_{lysis}n(t) \quad \text{(Equation 4)}$$

$$\frac{dGFP}{dt} = G_{max}F_G(AHL) - G_{deg}GFP(t) \quad \text{(Equation 5)}$$

$$F_A(AHL) = \frac{AHL(t)^m}{AHL_{th}^m + AHL(t)^m} \quad \text{(Equation 6)}$$

$$F_G(AHL) = \frac{AHL(t)^m}{GFP_{th}^m + AHL(t)^m} \quad \text{(Equation 7)}$$

Deterministic modeling of tetR-GFP synchronized oscillator dynamics

To model the behavior of the P2N1-Tet synchronized oscillator design, we used a delayed, ordinary differential equation model loosely based off a previous model of a similar synchronized oscillator (Danino et al., 2010). The model consists of two main equations describing the production and degradation of AHL (Equation 8) and TetR (Equation 9). Equation 8 takes into account that both the basal and maximal production rates of AHL are affected by TetR repression while basal AHL production leads to additional AHL production in an auto-catalytic positive feedback loop. Equation 9 takes into account that TetR expression is only impacted by AHL in the P2N1 design. To model the P2N2 design of the circuit, we replaced Equation 9 with Equation 10 to account for TetR negative autoregulation. In the model, the degradation terms for both AHL and TetR represent that both proteins are actively degraded by the same protease (ClpXP) via Michaelis-Menten kinetics. To account for delays in the transcription, translation, and production of AHL and TetR relative to their rapid binding to transcription factors or operator sites, we include a delay term (τ) in the hill functions for AHL and TetR (Equations 12 and 13). For modeling results looking at the impact of aTc (Figures S3D and S4E), we added a differential equation describing the binding of aTc to TetR (Equation 11). Since, aTc effectively prevents TetR from binding and repressing the pLuxTet promoter, we accounted for the effect of aTc in the hill function for TetR binding (Equation 12). All model results were obtained in MATLAB using the delayed differential equation solver, solveDDE. The following parameters were used in all of the synchronized oscillator model simulations except where noted: $A_0 = 5, T_0 = 2, A_{Max} = 30, T_{Max} = 5, AHL_{th} = 1, tetR_{th} = 1, m = 2, n = 4, A_{deg} = 1, T_{deg} = 1, f_{deg} = 0.1, \tau = 1, aTc = 0, K_c = 1000, K_d = 1$

$$\frac{dAHL}{dt} = A_0 F(tetR) + A_{max} F(AHL) F(tetR) - \frac{A_{deg} AHL(t)}{1 + f_{deg}(AHL(t) + tetR(t))} \quad \text{(Equation 8)}$$

$$\frac{dtetR}{dt} = T_0 + T_{max} F(AHL) - \frac{T_{deg} AHL(t)}{1 + f_{deg}(AHL(t) + tetR(t))} \quad \text{(Equation 9)}$$

$$\frac{dtetR}{dt} = T_0 F(tetR) + T_{max} F(AHL) F(tetR) - \frac{T_{deg} AHL(t)}{1 + f_{deg}(AHL(t) + tetR(t))} \quad \text{(Equation 10)}$$

$$\frac{dtetRaTc}{dt} = K_c [aTc]^2 (tetR(t) - tetRaTc(t)) - K_d tetRaTc(t) \quad \text{(Equation 11)}$$

$$F(tetR) = \frac{1}{1 + \left(\frac{tetR(t-\tau) - tetRaTc(t-\tau)}{tetR_{th}}\right)^m} \quad \text{(Equation 12)}$$

$$F(AHL) = \frac{AHL(t-\tau)^n}{AHL_{th}^n + AHL(t-\tau)^n} \quad \text{(Equation 13)}$$

QUANTIFICATION AND STATISTICAL ANALYSIS

All statistical details regarding replicates (n), mean, and standard deviation of particular data can be found in the relevant figure and figure caption. Throughout the manuscript, standard deviation is used a measure of experimental variability except where noted.